Numerical Simulation of Copper Temperature Field in Submerged Arc Welding (SAW) Process

Ali Moarrefzadeh

Department of Mechanical Engineering, Islamic Azad University, Mahshahr, Iran
a.moarefzadeh@mahshahriau.ac.ir

***Abstract*— Submerged Arc Welding (SAW) uses the arc struck between a continuously fed electrode and the work-piece to melt the metal in the joint area and provide additional filler metal under a blanket of granular flux. In this paper, the Submerged Arc Welding is studied and copper temperature field is gained in this process. The thermal effect of Submerged Arc that specially depends on the electrical arc, flux type and temperature field of it in work-piece, is the main key of analysis and optimization of this process, from which the main goal of this paper has been defined. Numerical simulation of welding process in SIMPELC method and by ANSYS software for gaining the temperature field of copper, the effect of parameter variation on temperature field and process optimization for different cases of Submerged Arc are done. The influence of the welding parameter for each mode on the dimensions and shape of the welds and on their ferrite contents is investigated.**

***Keywords*–** Numerical Simulation, Flux, SAW, FSI, SIMPLEC, Temperature Field and Copper

I. INTRODUCTION

Saw uses the arc struck between a continuously fed electrode and the work piece to melt the metal in the joint area and provide additional filler metal under a blanket of granular flux. This arc is completely submerged under the molten flux, which protects the molten metal from the atmosphere. There is no visible arc, spatter or fume during the welding operation.

The continuous electrode may be a solid or cored wire. The solid wires are normally copper coated. The cored wires may contain either metallic materials or a mixture of metallic and flux materials.

Flux cored wires affect the welding characteristics and metallurgical quality of the deposited weld metal. On surfacing applications, strip electrode can be used instead of a wire.

A wide range of flux compositions is used with submerged arc welding. Generally speaking, fluxes with the best welding characteristics give inferior weld metal mechanical properties. These fluxes are known as acid fluxes. Neutral fluxes generally give a good all round performance.

While basic fluxes give the best metallurgical results, they possess inferior welding characteristics. The normal approach is to select the flux with the best running characteristics that will meet the metallurgical requirements comfortably. SAW may be carried out using either DC or AC power sources. The best all round welding conditions are normally obtained with DC electrode positive. DC electrode negative will give higher deposition rates, but fusion characteristics are reduced so that this mode of transfer is mainly used on weld surfacing applications. AC welding may also be used, but arc control is not as good as on DC electrode positive. This means that many fluxes are developed primarily for DC operation and will not operate satisfactorily on AC.

Voltage controls the arc length and this has a major influence on the shape of the weld and its exterior appearance. Raising the arc voltage increases the arc length and this, in turn, increases the weld width. Lowering the arc voltage has the opposite effect. The travel speed controls the heat input into the joint area. Increasing travel speed reduces the heat input and supplies less filler metal per unit length of weld, resulting in less weld reinforcement.

Increasing travel speed reduces weld penetration but can cause undercut. Reducing travel speed provides time for the gases to escape from the molten metal and thus porosity may be reduced. Electrode "stick out", the distance between the contact tube and the arc, has a major affect on weld penetration and deposition rate. Increasing the "stick out" increases deposition rate and reduces weld penetration. However, to maintain optimum process control, the electrode "stick out" is normally maintained between 25–35 mm unless special nozzle adapters are fitted. SAW Process shows in Fig.1.

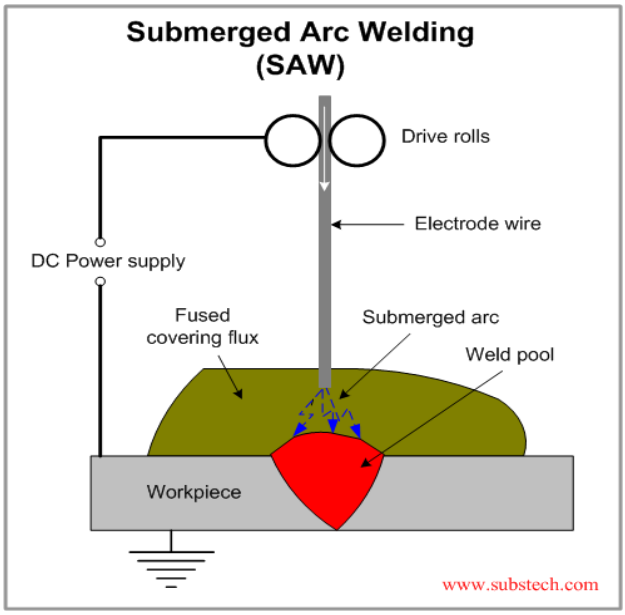

Fig. 1: Submerged Arc Welding (SAW) Process

II. GOVERNING EQUATIONS

In the common direct current electrode positive (DCEP) connection, the electrode is the anode and the workpiece is the cathode. A plasma arc is struck between the electrode and the workpiece. The electrode is continuously fed downward and melts at the tip by the high temperature arc. Droplets are then detached from the electrode and transferred to the workpiece. The computational domain includes an anode zone (electrode), an arc zone, and a cathode zone (workpiece). The anode and cathode sheaths have been omitted and treated as special boundary conditions for computational simplifications. Assuming the arc is in local thermal equilibrium (LTE) and the plasma flow is laminar and incompressible, the differential equations governing the arc, the electrode, detached droplet, and the workpiece can be put into a single set.

The differential equations governing the conservations of mass, momentum, and energy based on continuum formulation given by Chiang and Tsai are modified and employed in this study. The derivation of the equations can be found in The idea of continuum formulation is to eliminate the need of explicitly tracking the solidifying or melting interface, and therefore the established conversation equations is valid for both solid and liquid phases[2].

The differential Equations (1) – (8) are solved iteratively by the SIMPLEC numerical procedure:

Mass continuity equation:

$$\frac{1}{r}\frac{\partial}{\partial r}(r\rho v_r)+\frac{\partial}{\partial z}(\rho v_z)=0 \tag{1}$$

Radial momentum conservation equation:

$$\frac{1}{r}\frac{\partial}{\partial r}(r\rho v_r^2)+\frac{\partial}{\partial z}(\rho v_r v_z)= -\frac{\partial \rho}{\partial r}-j_z B_\theta+\frac{1}{r}\frac{\partial}{\partial r}(2r\eta\frac{\partial v_r}{\partial r})+ \frac{\partial}{\partial z}(\eta\frac{\partial v_r}{\partial z}+\eta\frac{\partial v_z}{\partial r})-2\eta\frac{v_r}{r^2} \tag{2}$$

Axial momentum conservation equation:

$$\frac{1}{r}\frac{\partial}{\partial r}(r\rho v_r v_z)+\frac{\partial}{\partial z}(\rho v_z^2)= -\frac{\partial \rho}{\partial z}+j_r B_\theta+\frac{\partial}{\partial z}(2\eta\frac{\partial v_z}{\partial z})+ \frac{1}{r}\frac{\partial}{\partial r}(r\eta\frac{\partial v_r}{\partial z}+r\eta\frac{\partial v_z}{\partial r}). \tag{3}$$

Energy conservation equation:

$$\frac{1}{r}\frac{\partial}{\partial r}(r\rho v_r h)+\frac{\partial}{\partial z}(\rho v_z h)= \frac{1}{r}\frac{\partial}{\partial r}(\frac{rk}{c_p}\frac{\partial h}{\partial r})+\frac{\partial}{\partial z}(\frac{k}{c_p}\frac{\partial h}{\partial z})+ j_r E_r+j_z E_z-R, \tag{4}$$

Conservation of thermal energy:

$$\frac{\partial}{\partial t}(\rho C_p T)+\frac{u}{r}\frac{\partial}{\partial r}(\rho C_p rT)+w\frac{\partial}{\partial z}(\rho C_p T) =\frac{1}{r}\frac{\partial}{\partial r}(kr\frac{\partial T}{\partial r})+\frac{\partial}{\partial Z}(K\frac{\partial T}{\partial Z})-\frac{\Delta H}{C_P}\frac{\partial F_L}{\partial t} \tag{5}$$

Conservation of electrical charge:

$$\mathbf{1}\frac{\partial}{\partial \mathrm{r}}(\sigma \mathrm{r}\frac{\partial \phi}{\partial \mathrm{r}})+\frac{\partial}{\partial \mathrm{z}}(\sigma\frac{\partial \phi}{\partial \mathrm{z}})=\mathbf{0} \tag{6}$$

Current continuity equation:

$$\frac{1}{r}\frac{\partial}{\partial r}(rj_r)+\frac{\partial}{\partial z}(j_z)=0, \tag{7}$$

Ohm's law:

$$j_r=-\sigma E_{r,} j_z=-\sigma E_{z,} \tag{8}$$

Where μ_0 is the permeability of free space.

In the solution of Equation (1) – (6), special attention needs to be put on the energy effects on the electrode surface. At the cathode surface, additional energy flux terms should be included in Eq. (4) because of thermionic cooling due to the mission of electrons, ion heating, and radiation cooling [2].

III. NUMERICAL SIMULATION

Finite elements simulations are done in 3 steps with the main pieces:

1- Modeling by FEMB
2- The thermal study and processing
3- Post-Processing result of analysis by ANSYS software for results discussion

Finite-Element techniques:

1-Finite elements modeling, types and properties for model different parts.
2- The definition of material properties
3- parameter definition
4- Loading
5- Boundary and initial value definition

IV. ELABORATION OF A MATHEMATICAL MODEL FOR MELTING RATE

Influences of welding parameters on melting rate in single wire and twin wire submerged arc welding were studied during numerous experiments. Melting rate depends mostly on welding current intensity, polarity, the electrode diameter and the wire extension length. In multiple-wire electrode welding, it depends also on the number of wires applied and the distance between them. The other welding parameters, i.e. welding speed, arc voltage, kind of shielding medium, type of welding current source, chemical composition of the filler material (valid for low-alloy steels) etc., have little influence. The majority of these parameters have been studied, their influence is known and in our judgment, they may be neglected.

A study of the influence of current intensity on melting rate was carried out by means of practical experiments. The results obtained are shown in Figs. 2 and 3. Fig. 2 shows the influence of welding current on melting rate in welding with a single wire and a twin wire having a diameter of 3 mm. Welding was carried out also with wire diameters of 1.2, 1.6 and 2.0 mm. The results for the twin wire are shown in Fig. 2 (L is the wire extension length and b is the distance between the wires). Based on both diagrams (Figs. 2 and 3) similar conclusions may be drawn. In all cases the melting rate increases slightly exponentially with an increase in welding current intensity.

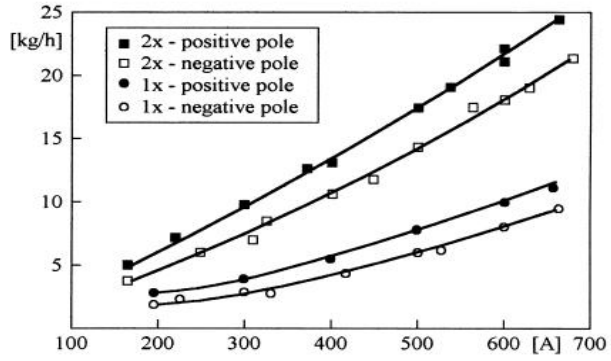

Fig. 2: Melting Rate Depending on Welding Current Intensity per Wire and on Polarity of a wire having a Diameter of 3 mm; L.30 mm, b.8 mm

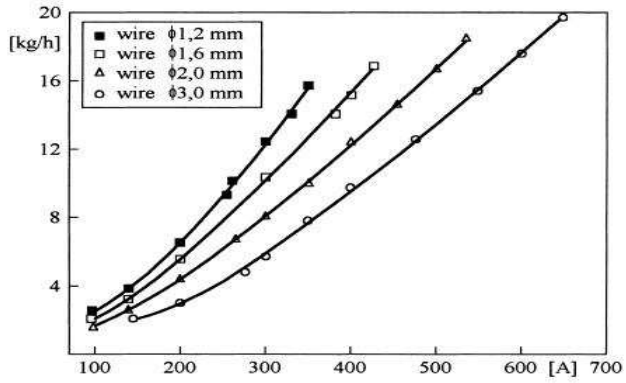

Fig. 3: Influence of Welding Current Intensity on the Melting Rate in Twin Electrode arc Welding with the following wire Diameters: 1.2, 1.6, 2.0 and 3.0 mm; L.25 mm, b.8 mm, U.30 V, Electrode Positive

V. NUMERICAL CONSIDERATIONS

For the metal domain, the method developed by Torrey et al. was used to solve p, u, v, and T. This method is Eulerian and allows for an arbitrary number of segments of free surface with any reasonable shape. The basic procedure for advancing the solution through one time step, Dt, consists of three steps. First, explicit approximations to the momentum Equations (2) – (4) are used to find provisional values of the new time velocities at the beginning of the time step. Second, an iterative procedure is used to solve for the advanced time pressure and velocity fields that satisfy Eq. (1) to within a convergence criterion at the new time. Third, the energy equation Eq. (5) is solved. Fig.3. shows A typical sequences of temperature, electrical potential, and pressure distributions on the symmetric plane for an axisymmetric stationary arc.

For the arc plasma domain, a fully implicit formulation is used for the time-dependent terms, and the combined convection/ diffusion coefficients are evaluated using an upwind scheme. The SIMPLEC algorithm is applied to solve the momentum and continuity Equations (1) – (5) to obtain the velocity field. At each time step, the current continuity equation Eq. (6) is solved first, based on the updated parameters.

The new distributions of current density and electromagnetic force are then calculated for the momentum and energy equations. The momentum equations and the mass continuity equation are then solved in the iteration process to obtain pressure and velocity. The energy equation is solved to get the new temperature distribution. Next, the temperature-dependent parameters are updated, and the program goes back to the first step to calculate the current continuity equation. This process is repeated for each time step until the convergence criteria are satisfied [2].

A study of the influence of the electrode diameter on melting rate substitutes, with some authors, for a study of the influence of welding current density. This substitution is possible in order to perform a super®cial estimation, but in an accurate analysis, particularly in submerged arc welding, such a substitution is not allowable. Welding current is conducted through the wire extension also on its surface. In submerged arc welding, where the wire is dipped into flux during welding, this plays an important part. The experimental results regarding the influence of the electrode diameter on melting rate are shown in Figs. 3 and 4. Even an inaccurate estimation of the influence of the electrode diameter on the melting rate shows that this is a rational fractional function and that the number of wires used has no important influence on the form of functional relation. In twin-wire electrode welding (3 mm wire), melting rate is by 30±35% lower than with a 1.2 mm wire with equal current intensity per wire.

VI. RESULTS AND DISCUSSION

Conclusions for fluid temperature field copper temperature field, completely shown in Fig.4.

a)

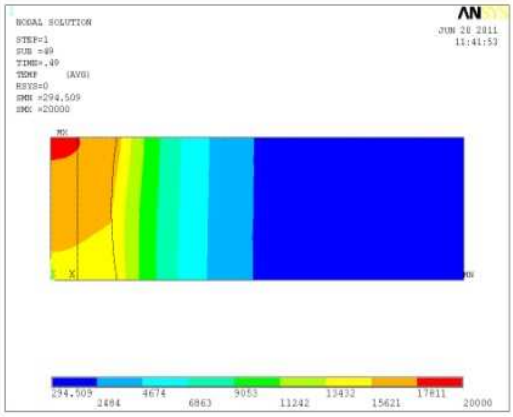

b)

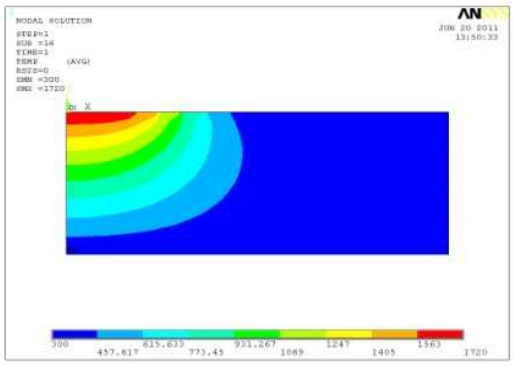

Fig. 4: Conclusions for Temperature Field: a) Temperature Field b) Copper Temperature Field

A complete 3D mathematical model for the SAW process is developed, the complete solution for a 3D case can be obtained if the numerical solution procedures proposed by Hu and Tsai are followed. The biggest challenge for such a 3D solution lies in the cost of numerical computation. Normally, the plasma flow can be computed with a relatively large grid size, but the metal flow requires a much smaller grid size in order to resolve various body forces within the tiny droplet.

Hu and Tsai used 0.1 mm grid size and $5*10^{-5}$ s time steps in their computations [7]. It is almost impossible to use the same resolutions for the 3D model. For example, in this study, the grid size is 0.2 mm and the average time step is $5*10^{-5}$ s. The numerical computations showed that the 0.2 mm grid size was not small enough to accurately calculate the balance of the surface tension force and the strong electromagnetic force in the pendant droplet.

As it already takes hours to calculate one time step, it is impractical to further reduce grid size. Thus, simplifications must be made based on the interest of current study.

This study focuses on the evolvement of the 3D plasma arc during the metal transfer process in SAW. Therefore, the fluid flow and heat transfer inside the metal zone can be greatly simplified because they have little effect on the electric and magnetic fields in plasma arc. As plasma arc is greatly

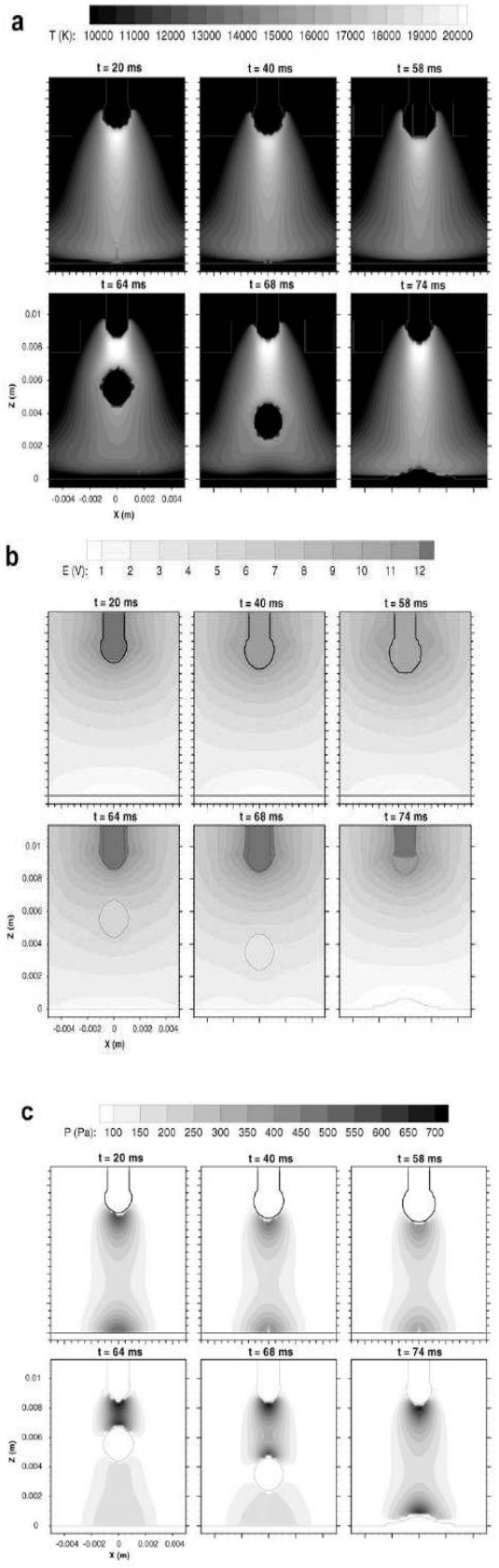

Fig. 5: A Typical Sequences of Temperature, Electrical Potential, and Pressure Distributions on the Symmetric Plane (y = 0) for an Axisymmetric Stationary arc: (a) Temperature, (b) Electrical Potential, (c) Pressure

affected by the topology of the metal zone and slightly affected by the temperature of the metal zone, tracking the topology of the metal zone by VOF method is more important for the model. Thus, the coupling of the plasma arc zone with the metal zone is relaxed by reducing the calculation of the plasma arc from at each time step to at some moments of interest. Fig.5. shows the distributions at the workpiece surface at t = 64 ms [3].

In this study, the electrode is a 1.6-mm- diameter mild steel wire and the workpiece is a 5-mm-thick mild steel chunk. The properties of steel are taken from in the computation. The shielding gas is argon (Ar). The welding current is 240 A and the equilibrium arc length is 9 mm. The electrode feed rate is set as 4.8 mm/s according to experiments in. The growth of the pendant droplet is controlled by the surface tension force only. This approximation reduces the complexities caused by the strong electromagnetic force, which requires smaller grid size and time step [3].

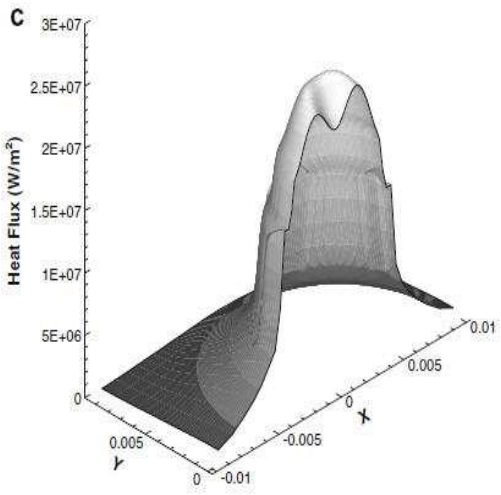

Fig. 6: Distributions at the Work-piece Surface at t = 64 ms: (a) Pressure, (b) Temperature, (c) Heat-Flux

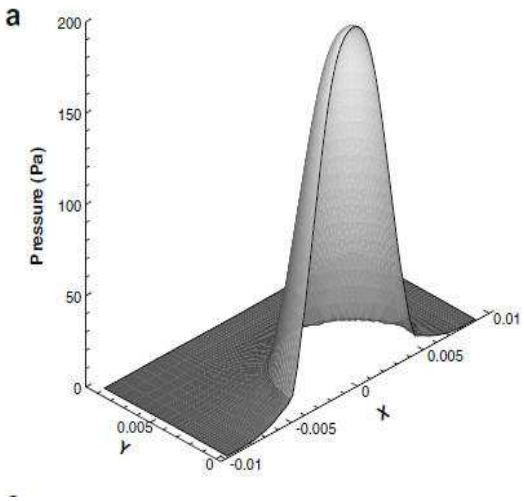

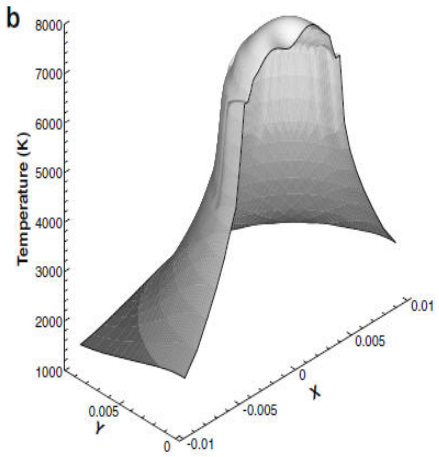

The droplet is artificially detached from the electrode with the presumed frequency. The period is 60 ms and the temperature of droplet is set as 3000 K according to Hu and Tsai. Although this droplet generation mechanism is simplified, reasonable results were obtained. The generated droplet is approximately in a sphere shape similar to that from the experimental observations.

The diameter of the generated droplet is determined by the electrode feed rate. The flight of the droplet to the workpiece is subject to the plasma drag force calculated by Eq. (6). This approximation is fairly good because the calculated droplet flight time is 12 ms for a 6 mm distance while the experimental measurement is about 12.5 ms when the initial axial droplet velocity is set as 0.28 m/s according to the experiments. It should be noted if the plasma flow is solved at every time step, then this approximation is not necessary and the drag force can be directly calculated from the plasma flow. The impingement of the droplet onto the workpiece is modeled using the aforementioned governing equations and boundary conditions.

However, the effects of arc pressure, plasma drag force, electromagnetic force, and arc heat flux on the workpiece are ignored because the plasma flow is not solved at every time step. This simplification is acceptable because at the moment of impingement, the momentum and energy carried by the droplet is much greater that those from the plasma arc. This simplification is supported by the facts that some droplet impingement models were able to obtain good numerical results even with inaccurate boundary conditions. Hu et al. used 48% for the ratio of the droplet thermal energy to the total input energy transferred to the workpiece. During one droplet impinging period, approximately half of the energy to the weld is abruptly brought in by the droplet during a short moment, while another half is continuously brought in by the arc during the entire period. By raising the droplet temperature to a higher value, in this study, 3000 K, the heat brought in by the arc is partially considered. As this study focuses on the plasma flow instead of the weld pool dynamics, only one

droplet impinging onto the workpiece is simulated. Thus, it is fair to ignore the arc heat flux during the impinging process. Based on the abovementioned approximations, the growth, detachment, and impingement of one droplet in the stationary axisymmetric arc have been computed using this 3D model. Though this case can be done by a 2D model, it is studied first to verify this 3D model.

The famous ‘‘bell-shape” plasma arc is observed from the temperature distributions. The highest temperature of the arc column is around 20,000 K and is consistent with the numerical results from the 2D models and the experimental measurements for SAW arcs.

Before the detachment, the highest temperate decreases as the droplet grow. It changes from 20,256 K at 20 ms to 19,050 K at 40 ms and then to 18,280 K at 58 ms (2 ms before the detachment).

This decrement is resultant from the globular growth of the pendant droplet. As it grows bigger, its surface area becomes larger and consequently the current density diverges more and become smaller. The arc temperature is therefore reduced because the holmic heating from the current contributes most of the arc energy.

The arc temperature boosts up right after the droplet detachment and then falls down as the droplet goes away. The arc between the electrode and the detached droplet is somewhat equivalent to an arc that gradually changes its arc length. Apparently, the shorter arc has a higher arc temperature. The calculated highest arc temperature is 21,742 K at 64 ms, and 20,893 K at 68 ms.

IV. CONCLUSIONS

A more elaborate mathematical model than the one existing before was developed for calculation of melting rate in single-wire arc welding. Additionally a mathematical model for calculation of melting rate in twin-wire arc welding not known from the literature before was developed. On the basis of variation of validity of the mathematical models developed for single-wire and twin-wire arc welding it can be stated that the models are quite a true representation of the experimental results and that they are applicable to practical cases as well as to further research work.

The use of the grey-based Taguchi method to determine the SAW process parameters with consideration of multiple performance characteristics has been reported in this paper.

A 3D mathematical model for the metal transfer process in SAW was formulated in this article. A complete model describing the SAW welding process is developed, however, the computation of the transient solution of the complete model was prohibitively time-consuming and beyond the capability of the current PCs. In order to study the plasma arc interaction with metal during the metal transfer process, some simplifications have been made. A case of an axisymmetric arc was studied first using this 3D model for the verification purpose. The numerical results agreed well with the previous two-dimensional studies. A case of a moving arc was then computed to demonstrate the 3D capability of the model. The results revealed that the time-invariant Gaussian assumption for the distributions of the arc pressure, heat flux, and current density on the workpiece surface did not represent of the real situation. The calculated distributions for the moving arc were non-axisymmetric and the peaks shifted to the arc moving direction.

REFERENCES

[1] S. Tashiro, M. Tanak, L. Murph, and J. Lowke, "Prediction of energy source properties of free-burning arc" Welding Journal, March 2008, pp. 23-29.

[2] Moarrefzadeh, "Numerical simulation of temperature field by Plasma arc welding Process in stainless steel" IREMOS Journal, February 2010, pp.101-107.

[3] Moarrefzadeh, “Choosing Suitable shielding gas for thermal optimization of GTAW process, IREME Journal, Sep 2010.

[4] E. Gorman, “New developments and application in plasma welding”, Welding Journal, July 2004, pp. 547-556.

[5] Y. Wang, and Q. Chen, "On-line quality monitoring in Plasma arc welding” Journal of Materials Processing Technology, January 2005, pp. 270-274.

[6] H. Kyselica, "High–Frequency reversing arc switch for plasma welding of Aluminum" Welding Journal, May 2005, pp. 31-35.

[7] G. Langford, "Plasma keyhole arc welding of structural stainless steel joints” Welding Journal, Feb2005, pp.102-113

[8] ANSYS Help system, Analysis Guide & Theory Reference Ver. 9, 10

[9] H. Miller, "Automated GTA welding for aerospace fabrication", Welding Journal, June 2005, pp.439-501.

Ali Moarrefzadeh
Young Researchers Club,
Faculty member of Department of Mechanical Engineering, Mahshahr Branch, Islamic Azad University ,
Mahshahr , Iran
E-mail: a_moarrefzadeh@yahoo.com
a.moarefzadeh@mahshahriau.ac.ir
Tel: +989123450936